

SYMPOCNET: SOLVING OPTIMAL CONTROL PROBLEMS WITH APPLICATIONS TO HIGH-DIMENSIONAL MULTI-AGENT PATH PLANNING PROBLEMS*

TINGWEI MENG^{†‡}, ZHEN ZHANG^{†‡}, JÉRÔME DARBON^{†§}, AND GEORGE EM KARNIADAKIS^{†¶}

Abstract. Solving high-dimensional optimal control problems in real-time is an important but challenging problem, with applications to multi-agent path planning problems, which have drawn increased attention given the growing popularity of drones in recent years. In this paper, we propose a novel neural network method called SympOCnet that applies the Symplectic network to solve high-dimensional optimal control problems with state constraints. We present several numerical results on path planning problems in two-dimensional and three-dimensional spaces. Specifically, we demonstrate that our SympOCnet can solve a problem with more than 500 dimensions in 1.5 hours on a single GPU, which shows the effectiveness and efficiency of SympOCnet. The proposed method is scalable and has the potential to solve truly high-dimensional path planning problems in real-time.

Key words. deep neural networks, optimal control, path planning, physics-informed learning

AMS subject classifications. 49M99, 68T07

1. Introduction. Optimal control methods are widely applied in many practical problems, which include path planning [17, 83, 43, 25, 75, 59, 65], humanoid robot control [30, 34, 56, 36, 33, 26], and robot manipulator control [61, 48, 54, 63, 12]. With the increasing impact of drones in everyday tasks as well as specialized military tasks, the path planning problem of multiple drones has become increasingly important. However, it is challenging to model this problem using the optimal control formulation because the dimensionality is usually very high, causing difficulty in applying traditional numerical methods, such as the very accurate pseudospectral (PS) method [31, 32, 77, 80, 38], to solve it. For instance, for a multi-agent path planning problem with M drones, the motion of each drone has to be described by a state variable in \mathbb{R}^m , therefore the dimension of the corresponding optimal control problem will be Mm , which is huge when the number of drones M is large. Computational complexity of traditional numerical methods may scale exponentially with respect to the dimension, which makes the high-dimensional problems intractable. This is an open issue called “curse-of-dimensionality” (CoD) [7]. Hence, new approaches are required to tackle high-dimensional optimal control problems efficiently.

In literature, there are some algorithms for solving high-dimensional optimal control problems (or the corresponding Hamilton-Jacobi PDEs), which include optimization methods [18, 24, 21, 23, 15, 14, 87, 60, 55], max-plus methods [1, 2, 29, 35, 39, 67, 66, 68, 69], tensor decomposition techniques [28, 44, 86], sparse grids [10, 37, 53], polynomial approximation [51, 52], model order reduction [4, 57], optimistic planning [9], dynamic programming and reinforcement learning [13, 11, 3, 8, 89], as well as methods based on neural networks [5, 6, 27, 47, 42, 45, 46, 58, 73, 78, 81, 84, 62, 20, 22, 19,

*Submitted to the editors January 17, 2022.

Funding: This work was supported by OSD/AFOSR MURI grant FA9550-20-1-0358.

[†]Division of Applied Mathematics, Brown University, Providence, RI 02912, USA (tingwei_meng@brown.edu, zhen_zhang1@brown.edu, Jerome_Darbon@brown.edu, George_Karniadakis@Brown.edu).

[‡]Tingwei Meng and Zhen Zhang contributed equally to this work.

[§]Corresponding author.

[¶]School of Engineering, Brown University, Providence, RI 02912, USA.

71, 72, 49, 50, 74]. However, path planning problems are in general hard to solve and cannot be solved directly by applying most of the aforementioned algorithms. One difficulty comes from the state constraints given by the complicated environment. Therefore, solving high-dimensional optimal control problems with complicated state constraints is an important yet challenging open problem. The difficulty of high dimensionality can be avoided by solving the sequential path planning problem instead of the simultaneous planning problem [13, 11, 79]. The main idea of sequential planning is to assign for different drones different levels of priorities and then sequentially solve the low-dimensional path planning problem involving each drone according to its priority. However, sequential planning only provides a feasible solution to the original simultaneous planning problem, which may not be optimal. Hence, how to solve high-dimensional simultaneous planning problems with complicated state constraints is still an unsolved problem.

Recently, neural networks have achieved great success in solving high-dimensional PDEs and inverse problems and bear some promise in overcoming the CoD. We can make further progress if we take advantage of the knowledge about the underlying data generation process and encode such information in the neural network architectures and the loss functions [49, 88, 40, 70]. As a specific example, the physics-informed neural network (PINN), which was first introduced in [76], encodes physical information directly into the loss function of neural networks using the residuals of ODEs/PDEs and automatic differentiation. In this work, we leverage PINNs and propose a novel method using a Symplectic optimal control network called SympOCnet to solve high-dimensional optimal control problems. SympOCnet is designed based on the Symplectic network (SympNet), which is a neural network architecture proposed in [50] and is able to approximate arbitrary symplectic maps. In the original paper, SympNet is used to solve the inverse parameter identification problem by acting as a surrogate model for the data generation procedure. In this paper, we present a novel way to utilize SympNet for solving Hamiltonian ODEs in a forward manner. By applying the SympOCnet, we encode our knowledge about optimal control problems and Hamilton-Jacobi theory in the neural network. We then apply SympOCnet on multi-agent path planning problems and show its effectiveness and efficiency in solving high-dimensional problems. Specifically, we can solve a path planning problem involving 256 drones, which corresponds to a 512-dimensional optimal control problem.

The organization of this paper is given as follows. In Section 2, we briefly summarize some preliminary background which will be used in the paper, including Hamiltonian systems and symplectic maps in Section 2.1 and SympNet in Section 2.2. In Section 3, we present our proposed SympOCnet method for the optimal control problems without state constraints, which serves as a building block for the full version of the SympOCnet method. The full version is then introduced in Section 4, which is proposed for solving the optimal control problems with state constraints. To be specific, we propose four loss functions, which are compared in the numerical experiments. Our numerical experiments on multi-agent path planning problems are presented in Section 5. The first example in Section 5.1 is used to compare the four loss functions. The second example in Section 5.2 demonstrates the generalizability of our method when only partial data is available in the training process. Then, in Sections 5.3 and 5.4, we demonstrate the effectiveness and efficiency of SympOCnet on high-dimensional problems, with dimensions ranging from 64 to 512. A summary is provided in Section 6.

2. Preliminary background. In this paper, we solve optimal control problems with SympOCnet, a neural network with SympNet architecture and loss function given by the corresponding Hamiltonian ODEs. This section provides some mathematical materials used in the remainder of the paper. In Section 2.1, we provide a brief summary about symplectic maps, Hamiltonian ODEs and their relations. Then, in Section 2.2, we review the SympNet architectures. For more details regarding the theory and applications of symplectic methods, we refer the readers to [41].

2.1. Hamiltonian systems and symplectic maps.

DEFINITION 2.1 (Symplectic maps). *Let U be an open set in \mathbb{R}^{2n} . A differentiable map $\phi : U \rightarrow \mathbb{R}^{2n}$ is called symplectic if the Jacobian matrix $\nabla\phi$ satisfies*

$$(2.1) \quad \nabla\phi^T(\mathbf{z})J\nabla\phi(\mathbf{z}) = J \quad \forall \mathbf{z} \in \mathbb{R}^{2n},$$

where J is a matrix with $2n$ rows and $2n$ columns defined by

$$(2.2) \quad J := \begin{pmatrix} \mathbf{0} & I_n \\ -I_n & \mathbf{0} \end{pmatrix},$$

and I_n denotes the identity matrix with n rows and n columns.

The Hamiltonian ODE system is a dynamical system taking the form

$$\dot{\mathbf{z}}(s) = J\nabla H(\mathbf{z}(s)),$$

where J is the matrix defined in (2.2) and $H : U \rightarrow \mathbb{R}$ is a function called Hamiltonian. The Hamiltonian systems and symplectic maps are highly related to each other. To be specific, the Hamiltonian structure is preserved under the change of variable using any symplectic map. This result is stated in the following theorem.

THEOREM 2.2. [41, Theorem 2.8 on p. 187] *Let U and V be two open sets in \mathbb{R}^{2n} . Let $\phi : U \rightarrow V$ be a change of coordinates such that ϕ and ϕ^{-1} are continuously differentiable functions. If ϕ is symplectic, the Hamiltonian ODE system $\dot{\mathbf{z}}(s) = J\nabla H(\mathbf{z}(s))$ can be written in the new variable $\mathbf{w} = \phi(\mathbf{z})$ as*

$$(2.3) \quad \dot{\mathbf{w}}(s) = J\nabla\tilde{H}(\mathbf{w}(s)),$$

where the new Hamiltonian \tilde{H} is defined by

$$(2.4) \quad \tilde{H}(\mathbf{w}) = H(\mathbf{z}) = H(\phi^{-1}(\mathbf{w})) \quad \forall \mathbf{w} \in V.$$

Conversely, if ϕ transforms every Hamiltonian system to another Hamiltonian system by (2.3) and (2.4), then ϕ is symplectic.

Theorem 2.2 indicates that a symplectic map can transform a Hamiltonian ODE system to another system which is again Hamiltonian and potentially in a simpler form. This is the starting point of our proposed method. It is well known from literature that the optimal trajectory of an optimal control problem is related to a Hamiltonian ODE system under certain assumptions. Such systems may be solved more easily if written in the right coordinates. We propose to learn the corresponding coordinate transformation through a parameterized family of symplectic maps ϕ_θ , where θ represents the unknown parameters to be learned, and solve the Hamiltonian ODEs with new coordinates. The solution to the original problem can be obtained by mapping the trajectory back to original phase space through $\varphi_\theta = \phi_\theta^{-1}$.

2.2. Symplectic networks (SympNets). SympNet is a neural network architecture proposed in [50] to approximate symplectic transformations. There are different kinds of SympNet architectures. In this paper, we use the G-SympNet as the class of our symplectic transformation φ_θ . For other architectures, we refer the readers to [50].

Define a function $\hat{\sigma}_{K,\mathbf{a},\mathbf{b}}: \mathbb{R}^n \rightarrow \mathbb{R}^n$ by $\hat{\sigma}_{K,\mathbf{a},\mathbf{b}}(\mathbf{x}) := K^T(\mathbf{a} \odot \sigma(K\mathbf{x} + \mathbf{b}))$ for any $\mathbf{x} \in \mathbb{R}^n$, where σ is the activation function, and \odot denotes the componentwise multiplication. Here \mathbf{a}, \mathbf{b} are vectors in \mathbb{R}^l , K is a matrix with l rows and n columns. Any G-SympNet is an alternating composition of the following two parameterized functions:

$$(2.5) \quad \begin{aligned} \mathcal{G}_{up} \begin{pmatrix} \mathbf{x} \\ \mathbf{p} \end{pmatrix} &= \begin{pmatrix} \mathbf{x} \\ \mathbf{p} + \hat{\sigma}_{K,\mathbf{a},\mathbf{b}}(\mathbf{x}) \end{pmatrix} \quad \forall \mathbf{x}, \mathbf{p} \in \mathbb{R}^n, \\ \mathcal{G}_{low} \begin{pmatrix} \mathbf{x} \\ \mathbf{p} \end{pmatrix} &= \begin{pmatrix} \hat{\sigma}_{K,\mathbf{a},\mathbf{b}}(\mathbf{p}) + \mathbf{x} \\ \mathbf{p} \end{pmatrix} \quad \forall \mathbf{x}, \mathbf{p} \in \mathbb{R}^n, \end{aligned}$$

where the learnable parameters are the matrix K and the vectors $\mathbf{a}, \mathbf{b} \in \mathbb{R}^l$. The dimension l (which is the dimension of \mathbf{a}, \mathbf{b} as well as the number of rows in K) is a positive integer that can be tuned, called the width of SympNet. In [50], it is proven that G-SympNets are universal approximators within the family of symplectic maps. Note that it is easy to obtain the inverse map of a G-SympNet, since we have explicit formulas for \mathcal{G}_{up}^{-1} and \mathcal{G}_{low}^{-1} given as follows

$$(2.6) \quad \mathcal{G}_{up}^{-1} \begin{pmatrix} \mathbf{x} \\ \mathbf{p} \end{pmatrix} = \begin{pmatrix} \mathbf{x} \\ \mathbf{p} - \hat{\sigma}_{K,\mathbf{a},\mathbf{b}}(\mathbf{x}) \end{pmatrix}, \quad \mathcal{G}_{low}^{-1} \begin{pmatrix} \mathbf{x} \\ \mathbf{p} \end{pmatrix} = \begin{pmatrix} \mathbf{x} - \hat{\sigma}_{K,\mathbf{a},\mathbf{b}}(\mathbf{p}) \\ \mathbf{p} \end{pmatrix}.$$

3. SympOCnet for optimal control problems without state constraints.

In this section, we consider the following optimal control problem without state constraints

$$(3.1) \quad \begin{aligned} &\min \left\{ \int_0^T \ell(\mathbf{x}(s), \mathbf{v}(s)) ds : \mathbf{x}(0) = \mathbf{x}_0, \mathbf{x}(T) = \mathbf{x}_T, \dot{\mathbf{x}}(s) = \mathbf{v}(s) \in U \forall s \in (0, T) \right\} \\ &= \min \left\{ \int_0^T \ell(\mathbf{x}(s), \dot{\mathbf{x}}(s)) ds : \mathbf{x}(0) = \mathbf{x}_0, \mathbf{x}(T) = \mathbf{x}_T, \dot{\mathbf{x}}(s) \in U \forall s \in (0, T) \right\}, \end{aligned}$$

where $\mathbf{v}: [0, T] \rightarrow U$ is the control function taking values in the control set $U \subseteq \mathbb{R}^n$, $\mathbf{x}: [0, T] \rightarrow \mathbb{R}^n$ is the corresponding trajectory, and $\ell: \mathbb{R}^n \times U \rightarrow \mathbb{R}$ is called running cost.

It is well-known in the literature that the solution \mathbf{x} to the optimal control problem (3.1) satisfies the following Hamiltonian ODE system

$$(3.2) \quad \begin{cases} \dot{\mathbf{x}}(s) = \nabla_{\mathbf{p}} H(\mathbf{x}(s), \mathbf{p}(s)), & s \in [0, T], \\ \dot{\mathbf{p}}(s) = -\nabla_{\mathbf{x}} H(\mathbf{x}(s), \mathbf{p}(s)), & s \in [0, T], \end{cases}$$

where the function $H: \mathbb{R}^{2n} \rightarrow \mathbb{R}$ is called Hamiltonian defined by

$$(3.3) \quad H(\mathbf{x}, \mathbf{p}) = \sup_{\mathbf{v} \in U} \{ \langle \mathbf{v}, \mathbf{p} \rangle - \ell(\mathbf{x}, \mathbf{v}) \}, \quad \forall \mathbf{x}, \mathbf{p} \in \mathbb{R}^n.$$

A method to solve the optimal control problem (3.1) in high dimensions is to solve the corresponding Hamiltonian ODE system (3.2) instead. However, when the Hamiltonian is too complicated, the Hamiltonian ODEs may be hard to solve. To tackle this

difficulty, we propose a method called SympOCnet, which uses the SympNet architecture to solve the optimal control problem (3.1) in high dimensions. The key idea is to perform a change of variables in the phase space using a symplectic map represented by a SympNet, and then solve the Hamiltonian ODEs in the new coordinate system.

Given a symplectic map $\phi: \mathbb{R}^{2n} \rightarrow \mathbb{R}^{2n}$, we define the change of variables $(\mathbf{y}, \mathbf{q}) = \phi(\mathbf{x}, \mathbf{p})$ for any $\mathbf{x}, \mathbf{p} \in \mathbb{R}^n$. If the phase trajectory $t \mapsto (\mathbf{x}(t), \mathbf{p}(t))$ is the solution to the Hamiltonian ODEs (3.2), then by Theorem 2.2, the phase trajectory $t \mapsto (\mathbf{y}(t), \mathbf{q}(t))$ under the new coordinate system solves the Hamiltonian ODEs with a new Hamiltonian $\tilde{H}: \mathbb{R}^{2n} \rightarrow \mathbb{R}$ defined by

$$\tilde{H}(\mathbf{y}, \mathbf{q}) = H(\phi^{-1}(\mathbf{y}, \mathbf{q})) \quad \forall \mathbf{y}, \mathbf{q} \in \mathbb{R}^n.$$

In other words, the function $t \mapsto (\mathbf{y}(t), \mathbf{q}(t))$ satisfies

$$(3.4) \quad \begin{cases} \dot{\mathbf{y}}(s) = \nabla_{\mathbf{q}} \tilde{H}(\mathbf{y}(s), \mathbf{q}(s)), & s \in [0, T], \\ \dot{\mathbf{q}}(s) = -\nabla_{\mathbf{y}} \tilde{H}(\mathbf{y}(s), \mathbf{q}(s)), & s \in [0, T]. \end{cases}$$

Here, we assume that the new Hamiltonian \tilde{H} has a simpler form such that the corresponding Hamiltonian ODE system (3.4) is easier to solve. To be specific, we assume that \tilde{H} does not depend on the variable \mathbf{y} , and hence the Hamiltonian ODEs become

$$(3.5) \quad \begin{cases} \dot{\mathbf{y}}(s) = \nabla_{\mathbf{q}} \tilde{H}(\mathbf{q}(s)), & s \in [0, T], \\ \dot{\mathbf{q}}(s) = 0, & s \in [0, T]. \end{cases}$$

The solution $s \mapsto \mathbf{q}(s)$ is a constant function, and the solution $s \mapsto \mathbf{y}(s)$ is an affine function. Therefore, the solution $s \mapsto (\mathbf{y}(s), \mathbf{q}(s))$ can be represented using three parameters in \mathbb{R}^n , which are denoted by $\mathbf{q}_0 = \mathbf{q}(0)$, $\mathbf{y}_0 = \mathbf{y}(0)$ and $\mathbf{u} = \dot{\mathbf{y}}(s)$. With these three parameters, the solution to (3.5) is given by $\mathbf{y}(s) = \mathbf{y}_0 + s\mathbf{u}$ and $\mathbf{q}(s) = \mathbf{q}_0$ for any $s \in [0, T]$.

Under this framework, we explain our proposed method in the remainder of this section. In Section 3.1, we apply the SympOCnet method to approximate the unknown function ϕ and the unknown parameters \mathbf{u} , \mathbf{y}_0 and \mathbf{q}_0 . Then, after the training process, to further enhance the accuracy we can also apply the pseudospectral method for post-processing (for low-dimensional problems), as we explain in Section 3.2.

3.1. SympOCnet method. In this section, we describe how to apply SympOCnet method to solve the optimal control problem (3.1). SympOCnet uses a SympNet architecture to represent the inverse of the unknown function ϕ , which is also a symplectic map. In other words, we approximate ϕ^{-1} using a SympNet denoted by $\varphi = (\varphi_1, \varphi_2)$. Here, φ_1 denotes the first n components in φ , which is a map from (\mathbf{y}, \mathbf{q}) to \mathbf{x} , and φ_2 denotes the last n components in φ , which is a map from (\mathbf{y}, \mathbf{q}) to \mathbf{p} . Other learnable parameters include $\mathbf{u}, \mathbf{y}_0, \mathbf{q}_0 \in \mathbb{R}^n$ mentioned above, which respectively correspond to $\dot{\mathbf{y}}(s)$, $\mathbf{y}(0)$ and $\mathbf{q}(s)$ in the new Hamiltonian ODE system (3.5). With the SympNet φ and the variables $\mathbf{u}, \mathbf{y}_0, \mathbf{q}_0$, the solution to the original Hamiltonian ODEs (3.2) is given by $s \mapsto \varphi(\mathbf{y}_0 + s\mathbf{u}, \mathbf{q}_0)$.

To learn the SympNet φ and the parameters \mathbf{u}, \mathbf{y}_0 and \mathbf{q}_0 , we apply the PINN

loss [76] on the Hamiltonian ODEs (3.2), and get

$$\begin{aligned}\mathcal{L}_{res} &= \sum_{j=1}^N \left\| \frac{d\mathbf{x}(s_j)}{ds} - \nabla_{\mathbf{p}}H(\mathbf{x}(s_j), \mathbf{p}(s_j)) \right\|^2 + \sum_{j=1}^N \left\| \frac{d\mathbf{p}(s_j)}{ds} + \nabla_{\mathbf{x}}H(\mathbf{x}(s_j), \mathbf{p}(s_j)) \right\|^2 \\ &= \sum_{j=1}^N \left\| \nabla_{\mathbf{y}}\varphi_1(\mathbf{y}_0 + s_j\mathbf{u}, \mathbf{q}_0)\mathbf{u} - \nabla_{\mathbf{p}}H(\varphi(\mathbf{y}_0 + s_j\mathbf{u}, \mathbf{q}_0)) \right\|^2 \\ &\quad + \sum_{j=1}^N \left\| \nabla_{\mathbf{y}}\varphi_2(\mathbf{y}_0 + s_j\mathbf{u}, \mathbf{q}_0)\mathbf{u} + \nabla_{\mathbf{x}}H(\varphi(\mathbf{y}_0 + s_j\mathbf{u}, \mathbf{q}_0)) \right\|^2,\end{aligned}$$

where the second equality holds by the following chain rule

$$\begin{aligned}\frac{d\mathbf{x}(s_j)}{ds} &= \nabla_{\mathbf{y}}\mathbf{x}(\mathbf{y}_0 + s_j\mathbf{u}, \mathbf{q}_0)\frac{d\mathbf{y}(s_j)}{ds} + \nabla_{\mathbf{q}}\mathbf{x}(\mathbf{y}_0 + s_j\mathbf{u}, \mathbf{q}_0)\frac{d\mathbf{q}(s_j)}{ds} \\ &= \nabla_{\mathbf{y}}\varphi_1(\mathbf{y}_0 + s_j\mathbf{u}, \mathbf{q}_0)\mathbf{u}, \\ \frac{d\mathbf{p}(s_j)}{ds} &= \nabla_{\mathbf{y}}\mathbf{p}(\mathbf{y}_0 + s_j\mathbf{u}, \mathbf{q}_0)\frac{d\mathbf{y}(s_j)}{ds} + \nabla_{\mathbf{q}}\mathbf{p}(\mathbf{y}_0 + s_j\mathbf{u}, \mathbf{q}_0)\frac{d\mathbf{q}(s_j)}{ds} \\ &= \nabla_{\mathbf{y}}\varphi_2(\mathbf{y}_0 + s_j\mathbf{u}, \mathbf{q}_0)\mathbf{u}.\end{aligned}$$

Here, the data points are given by $s_1, \dots, s_N \in [0, T]$. The gradients $\nabla_{\mathbf{y}}\varphi_1(\mathbf{y}_0 + s_j\mathbf{u}, \mathbf{q}_0)$ and $\nabla_{\mathbf{y}}\varphi_2(\mathbf{y}_0 + s_j\mathbf{u}, \mathbf{q}_0)$ are calculated by the automatic differentiation of the SympNet φ . Moreover, we have another loss term for the initial and terminal conditions of \mathbf{x} , defined by

$$\begin{aligned}\mathcal{L}_{bd} &= \|\mathbf{x}(0) - \mathbf{x}_0\|^2 + \|\mathbf{x}(T) - \mathbf{x}_T\|^2 \\ &= \|\varphi_1(\mathbf{y}_0, \mathbf{q}_0) - \mathbf{x}_0\|^2 + \|\varphi_1(\mathbf{y}_0 + T\mathbf{u}, \mathbf{q}_0) - \mathbf{x}_T\|^2.\end{aligned}$$

The total loss function \mathcal{L} is a weighted sum of the two loss terms, defined by

$$(3.6) \quad \mathcal{L} = \mathcal{L}_{res} + \lambda\mathcal{L}_{bd},$$

where λ is a tunable positive hyperparameter. After training, the optimal trajectory is obtained from

$$(3.7) \quad \mathbf{x}(s) = \varphi_1(\mathbf{y}_0 + s\mathbf{u}, \mathbf{q}_0) \quad \forall s \in [0, T],$$

where the function φ_1 contains the first n components of the SympNet φ . An illustration of our proposed SympOCnet method is shown in Figure 1.

3.2. Post-processing using the pseudospectral method. In Section 3.1, we introduced the SympOCnet to solve the optimal control problem (3.1). In this section, we explain how to apply the pseudospectral method to postprocess SympOCnet results to improve feasibility and optimality. The pseudospectral method is a popular method proposed to solve a general optimal control problem [31, 32, 77, 80, 38]. It applies the quadrature rule to discretize the integration and the ODE in a continuous optimal control problem. In this way, the continuous optimal control problem is converted to a finite-dimensional optimization problem with constraints. Then, some optimization algorithms such as sequential quadratic programming are applied to solve the finite-dimensional problem.

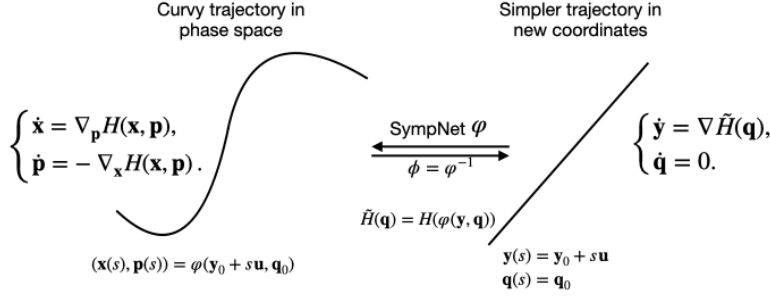


Fig. 1: **An illustration of the SympOCnet method.** We propose to use SympNet ϕ to map curvy trajectory in the phase space to simpler trajectory in new coordinates and solve the corresponding Hamiltonian system of the optimal control problem.

When the dimension is high, it is, in general, hard to solve the converted finite-dimensional optimization problem. The difficulty comes from the number of variables and constraints in the optimization problem, as well as the non-convexity of the problem. However, there are some theoretical guarantees when the initialization is good enough. Therefore, it can be applied as a postprocessing procedure by taking the trajectory obtained from Section 3.1 as an initialization.

We will apply this procedure in the numerical experiments in Sections 5.1 and 5.2. From the numerical results, we observe that the pseudospectral method preserves the shape of the trajectories obtained from the training step of the SympOCnet method, and it makes the trajectories smoother while improving the optimality. Therefore, the pseudospectral method performs well as a post-processing method. It is also observed in the experiments that pseudospectral method itself with a linear initialization may not converge to the correct solution, which justifies the choice of SympOCnet as a good initializer. Note that we do not apply this post-process to the experiments in Sections 5.3 and 5.4 due to the high dimensionality.

4. SympOCnet for optimal control problems with state constraints. In this section, we focus on the following optimal control problem with state constraints

$$\begin{aligned}
 & \min \left\{ \int_0^T \ell(\mathbf{x}(s), \mathbf{v}(s)) ds : h(\mathbf{x}(s)) \geq 0, \dot{\mathbf{x}}(s) = \mathbf{v}(s) \in U \forall s \in [0, T], \right. \\
 & \qquad \qquad \qquad \left. \mathbf{x}(0) = \mathbf{x}_0, \mathbf{x}(T) = \mathbf{x}_T \right\} \\
 (4.1) \quad & = \min \left\{ \int_0^T \ell(\mathbf{x}(s), \dot{\mathbf{x}}(s)) ds : h(\mathbf{x}(s)) \geq 0, \dot{\mathbf{x}}(s) \in U \forall s \in [0, T], \right. \\
 & \qquad \qquad \qquad \left. \mathbf{x}(0) = \mathbf{x}_0, \mathbf{x}(T) = \mathbf{x}_T \right\},
 \end{aligned}$$

where $\ell: \mathbb{R}^n \times U \rightarrow \mathbb{R}$ is the running cost, and $h: \mathbb{R}^n \rightarrow \mathbb{R}^m$ is a function providing the constraint on the state variable \mathbf{x} . For instance, to avoid obstacles, h can be defined using the signed distance function to the obstacles.

In order to apply the SympOCnet method in Section 3, we need to convert the

original problem (4.1) to an unconstrained optimal control problem, which is achieved using the soft penalty method described in Section 4.1. The soft penalty method will enforce the constraints in an asymptotic sense, i.e., when the hyperparameters converge to zero under some conditions, which is impractical in experiments. In the training process, when the hyperparameters in the soft penalty are fixed, to improve the feasibility of the output trajectory, we introduce extra terms in the loss function in Sections 4.2 and 4.3. The selection of these extra loss terms may differ from problem to problem. Later in Section 5.1, we compare the performance of different loss functions under our path planning problem setup to choose a suitable loss function for the other experiments.

4.1. Soft penalty method for the optimal control problem. To convert a constrained problem to an unconstrained one, the soft penalty method replaces the hard constraint by a soft penalty term in the objective function. Here, we consider the log penalty function [82, 85], denoted by $\beta_a: \mathbb{R} \rightarrow \mathbb{R}$ and defined by

$$(4.2) \quad \beta_a(x) := \begin{cases} -\log(x), & \text{if } x > a, \\ -\log(a) + \frac{1}{2} \left(\left(\frac{x-2a}{a} \right)^2 - 1 \right), & \text{if } x \leq a, \end{cases}$$

where a is a positive hyperparameter. The high-dimensional log penalty function is the summation of the one-dimensional function acting on each component, i.e., for any $m > 1$, the log penalty function $\beta_a: \mathbb{R}^m \rightarrow \mathbb{R}$ is defined by

$$(4.3) \quad \beta_a(\mathbf{x}) := \sum_{i=1}^m \beta_a(x_i) \quad \forall \mathbf{x} = (x_1, \dots, x_m) \in \mathbb{R}^m.$$

With this log penalty term, the problem (4.1) is converted to

$$(4.4) \quad \min \left\{ \int_0^T \ell(\mathbf{x}(s), \dot{\mathbf{x}}(s)) + \epsilon \beta_a(h(\mathbf{x}(s))) ds : \dot{\mathbf{x}}(s) \in U \forall s \in [0, T], \right. \\ \left. \mathbf{x}(0) = \mathbf{x}_0, \mathbf{x}(T) = \mathbf{x}_T \right\},$$

where ϵ and a are positive hyperparameters. This problem (4.4) is in the form of (3.1), and hence can be solved using the SympOCnet method in Section 3. By straightforward calculation, for a sequence of parameters ϵ_k and a_k such that they both converge to zero and the following equations hold

$$\lim_{k \rightarrow \infty} \epsilon_k \log a_k = 0, \quad \lim_{k \rightarrow \infty} \frac{a_k^2}{\epsilon_k} = 0,$$

the penalty term $\epsilon_k \beta_{a_k}$ converges to the indicator function of $[0, +\infty)$, which takes the value 0 in $[0, +\infty)$ and $+\infty$ in $(-\infty, 0)$. Therefore, the objective function in (4.4) with parameters ϵ_k , a_k converges to the objective function in (4.1) with the hard constraint given by h .

With this penalty term, the Hamiltonian corresponding to the optimal control problem (4.4) equals

$$(4.5) \quad H_{\epsilon, a}(\mathbf{x}, \mathbf{p}) = \sup_{\mathbf{v} \in U} \{ \langle \mathbf{v}, \mathbf{p} \rangle - \ell(\mathbf{x}, \mathbf{v}) - \epsilon \beta_a(h(\mathbf{x})) \} = H(\mathbf{x}, \mathbf{p}) - \epsilon \beta_a(h(\mathbf{x})),$$

where H is the Hamiltonian corresponding to the running cost ℓ defined in (4.4).

REMARK 1. Note that another widely-used method to convert a constrained optimization problem to an unconstrained one is the augmented Lagrangian method. In our problem, since the constraint is enforced for any time $s \in [0, T]$, to apply the augmented Lagrangian method, the Lagrange multiplier needs to be a function of time. Then, with the added Lagrangian term, the new running cost also depends on the time variable, which requires a more complicated symplectic method to handle time-dependent Hamiltonians. Therefore, we do not apply the augmented Lagrangian method for the constrained optimal control problem (4.1) in this paper. Instead, we add extra terms in the loss function (see Sections 4.2 and 4.3) to enforce the constraint.

4.2. Penalty method in the training process of SympOCnet. To enforce the state constraint $h(\mathbf{x}(s)) \geq 0$, one way is to add the penalty term in the loss function of the training process. Here, we introduce two penalty terms, which include the log penalty β_a defined in (4.3) and the quadratic penalty. The loss function with the log penalty term corresponding to the state constraint $h(\mathbf{x}(s)) \geq 0$ is defined by

$$(4.6) \quad \begin{aligned} \mathcal{L}_{\log}(\varphi, \mathbf{y}_0, \mathbf{q}_0, \mathbf{u}) &= \mathcal{L}(\varphi, \mathbf{y}_0, \mathbf{q}_0, \mathbf{u}) + \frac{\tilde{\lambda}}{N} \sum_{j=1}^N \epsilon \beta_a(h(\varphi_1(\mathbf{y}_0 + s_j \mathbf{u}, \mathbf{q}_0))) \\ &\quad + \epsilon \beta_a(\mathbf{x}_0 - \varphi_1(\mathbf{y}_0, \mathbf{q}_0)) + \epsilon \beta_a(\varphi_1(\mathbf{y}_0, \mathbf{q}_0) - \mathbf{x}_0) \\ &\quad + \epsilon \beta_a(\mathbf{x}_T - \varphi_1(\mathbf{y}_0 + T\mathbf{u}, \mathbf{q}_0)) + \epsilon \beta_a(\varphi_1(\mathbf{y}_0 + T\mathbf{u}, \mathbf{q}_0) - \mathbf{x}_T), \end{aligned}$$

where β_a is the penalty function defined in (4.3), \mathcal{L} is the loss function defined in Section 3.1, and $\tilde{\lambda}$ is a positive hyperparameter. Similarly, the loss function with a quadratic penalty is defined by

$$(4.7) \quad \mathcal{L}_{quad}(\varphi, \mathbf{y}_0, \mathbf{q}_0, \mathbf{u}) = \mathcal{L}(\varphi, \mathbf{y}_0, \mathbf{q}_0, \mathbf{u}) + \frac{\tilde{\lambda}}{N} \sum_{j=1}^N \|\min\{h(\varphi_1(\mathbf{y}_0 + s_j \mathbf{u}, \mathbf{q}_0)), 0\}\|^2,$$

where we do not add the penalty term for the initial and terminal conditions, since the quadratic penalty for them are the same with \mathcal{L}_{bd} in the loss function \mathcal{L} .

4.3. Augmented Lagrangian method in the training process of SympOCnet. Another method to enforce the state constraint $h(\mathbf{x}(s)) \geq 0$ is to apply augmented Lagrangian method in the training process. The loss function with the Lagrangian term is defined as follows

$$(4.8) \quad \begin{aligned} &\mathcal{L}_{aug}(\varphi, \mathbf{y}_0, \mathbf{q}_0, \mathbf{u}, \boldsymbol{\mu}, \boldsymbol{\lambda}_1, \boldsymbol{\lambda}_2) \\ &= \mathcal{L}(\varphi, \mathbf{y}_0, \mathbf{q}_0, \mathbf{u}) + \frac{1}{2\rho_1} \sum_{j=1}^N \|\max\{\mathbf{0}, \boldsymbol{\mu}(s_j) - \rho_1 h(\varphi_1(\mathbf{y}_0 + s_j \mathbf{u}, \mathbf{q}_0))\}\|^2 \\ &\quad + \frac{1}{2\rho_2} (\|\boldsymbol{\lambda}_1 - \rho_2(\mathbf{x}_0 - \varphi_1(\mathbf{y}_0, \mathbf{q}_0))\|^2 + \|\boldsymbol{\lambda}_2 - \rho_2(\mathbf{x}_T - \varphi_1(\mathbf{y}_0 + T\mathbf{u}, \mathbf{q}_0))\|^2), \end{aligned}$$

where $\boldsymbol{\mu}(s_j) \in \mathbb{R}^m$, $\boldsymbol{\lambda}_1, \boldsymbol{\lambda}_2 \in \mathbb{R}^n$ are the augmented Lagrange multipliers for the constraints $h(\mathbf{x}(s_j)) \geq 0$, $\mathbf{x}(0) = \mathbf{x}_0$ and $\mathbf{x}(T) = \mathbf{x}_T$, respectively, and $\rho_1, \rho_2 > 0$ are positive hyperparameters in the augmented Lagrangian method. The training process becomes an iterative scheme where the k -th iteration contains the following two steps

- Train the SympNet φ and parameters $\mathbf{y}_0, \mathbf{q}_0, \mathbf{u} \in \mathbb{R}^n$ for several iterations using the loss function $\mathcal{L}_{aug}(\varphi, \mathbf{y}_0, \mathbf{q}_0, \mathbf{u}, \boldsymbol{\mu}^k, \boldsymbol{\lambda}_1^k, \boldsymbol{\lambda}_2^k)$;

- Update the Lagrange multiplier by

$$\begin{aligned}\boldsymbol{\mu}^{k+1}(s_j) &= \max\{\mathbf{0}, \boldsymbol{\mu}^k(s_j) - \rho_1 h(\varphi_1(\mathbf{y}_0 + s_j \mathbf{u}, \mathbf{q}_0))\} \quad \forall j = 1, \dots, N, \\ \boldsymbol{\lambda}_1^{k+1} &= \boldsymbol{\lambda}_1^k - \rho_2(\mathbf{x}_0 - \varphi_1(\mathbf{y}_0, \mathbf{q}_0)), \\ \boldsymbol{\lambda}_2^{k+1} &= \boldsymbol{\lambda}_2^k - \rho_2(\mathbf{x}_T - \varphi_1(\mathbf{y}_0 + T\mathbf{u}, \mathbf{q}_0)).\end{aligned}$$

Note that in practice, we need to tune the hyperparameters ρ_1 and ρ_2 . In our implementation, these hyperparameters are tuned automatically using a similar strategy as in [16].

5. Applications in path planning problems with obstacle and collision avoidance. In this section, we apply our method to path planning problems with multiple drones. We assume that each drone is represented by a ball in the physical space \mathbb{R}^m with radius C_d . Note that the meaning of the notation m in this section (i.e., the dimension of the physical space) is different from m in Section 4 (which is the number of state constraints). We set the state variable to be $\mathbf{x} = (\mathbf{x}_1, \dots, \mathbf{x}_M) \in \mathbb{R}^{Mm}$, where M is the number of drones, and each $\mathbf{x}_j \in \mathbb{R}^m$ denotes the position of the center of each drone. In other words, the state variable is the concatenation of the position variables of all drones. Similarly, the control variable \mathbf{v} is the concatenation of the velocity variables for all drones, i.e., \mathbf{v} equals $(\mathbf{v}_1, \dots, \mathbf{v}_M) \in U^M$, where each \mathbf{v}_j is the velocity of the j -th drone, and $U \subseteq \mathbb{R}^m$ is the space for all admissible velocities for each drone. In our numerical experiments, the control space U is the ball in \mathbb{R}^m with zero center and radius $C_v > 0$, i.e., the norm of the velocity of each drone has the upper bound C_v .

We want to solve for the optimal trajectory with minimal energy, and hence the running cost is set to be

$$\ell(\mathbf{x}, \mathbf{v}) = \frac{1}{2} \|\mathbf{v}\|^2 \quad \forall \mathbf{x} \in \mathbb{R}^{Mm}, \mathbf{v} \in U^M.$$

The corresponding Hamiltonian equals

$$\begin{aligned}H(\mathbf{x}, \mathbf{p}) &= \sup_{\mathbf{v} \in U^M} \left\{ \langle \mathbf{v}, \mathbf{p} \rangle - \frac{1}{2} \|\mathbf{v}\|^2 \right\} = \sum_{i=1}^M \sup_{\mathbf{v}_i \in U} \left\{ \langle \mathbf{v}_i, \mathbf{p}_i \rangle - \frac{1}{2} \|\mathbf{v}_i\|^2 \right\} \\ &= \sum_{i=1}^M \begin{cases} \frac{1}{2} \|\mathbf{p}_i\|^2 & \text{if } \|\mathbf{p}_i\| \leq C_v, \\ C_v \|\mathbf{p}_i\| - \frac{C_v^2}{2} & \text{if } \|\mathbf{p}_i\| > C_v, \end{cases}\end{aligned}$$

for any $\mathbf{p} = (\mathbf{p}_1, \dots, \mathbf{p}_M) \in \mathbb{R}^{Mm}$, where each \mathbf{p}_i is the momentum variable in \mathbb{R}^m for the i -th drone.

To avoid obstacles and collisions among drones, we set the constraint function h to be $h = (h_1, h_2)$, where h_1 is for obstacle avoidance, and h_2 is for avoiding collisions among drones. If there are n_o obstacles, denoted by E_1, \dots, E_{n_o} , then the function $h_1: \mathbb{R}^{Mm} \rightarrow \mathbb{R}^{Mn_o}$ is defined by

$$(5.1) \quad h_1(\mathbf{x}_1, \dots, \mathbf{x}_M) = (d(\mathbf{x}_1), d(\mathbf{x}_2), \dots, d(\mathbf{x}_M)) \quad \forall \mathbf{x}_1, \dots, \mathbf{x}_M \in \mathbb{R}^m,$$

where the function $d: \mathbb{R}^m \rightarrow \mathbb{R}^{n_o}$ is defined by

$$(5.2) \quad d(\mathbf{x}) = (d_1(\mathbf{x}), \dots, d_{n_o}(\mathbf{x})) \quad \forall \mathbf{x} \in \mathbb{R}^m,$$

and each function d_j is defined such that $d_j(\mathbf{x}) < 0$ implies the collision of the drone whose center is at the position \mathbf{x} with the j -th obstacle E_j . For instance, d_j can be defined using the signed distance function to E_j . The definition of the function d_j depends on the shape of the constraint set E_j , and hence we do not specify it now but postpone its definition to each example in later sections.

The function $h_2: \mathbb{R}^{Mm} \rightarrow \mathbb{R}^{M(M-1)/2}$ is the constraint function for collision avoidance; each component of the constraint function gives a constraint for avoiding collision between a pair of drones. Since each drone can be seen as a ball centered at a point in \mathbb{R}^m , two drones collide if and only if the distance between their centers is less than the sum of their radii. Hence, we set the k -th component of h_2 to be

$$(5.3) \quad (h_2)_k(\mathbf{x}_1, \dots, \mathbf{x}_M) = \|\mathbf{x}_i - \mathbf{x}_j\|^2 - (2C_d)^2 \quad \forall \mathbf{x}_1, \dots, \mathbf{x}_M \in \mathbb{R}^m,$$

where C_d is the radius of a drone, and $k = i + (j-1)(j-2)/2$ for any $1 \leq i < j \leq M$ is the corresponding constraint index for the pair (i, j) . Note that the constraints may be duplicated to simplify the implementation. As a result, $(h_2)_k(\mathbf{x}_1, \dots, \mathbf{x}_M) < 0$ is equivalent to the collision between the i -th and j -th drones. In other words, such defined constraint function h_2 can avoid collisions among drones.

In the following sections, we present several numerical results. In Section 5.1, we compare the performance of different loss functions \mathcal{L} , \mathcal{L}_{log} , \mathcal{L}_{quad} and \mathcal{L}_{aug} to choose a suitable loss function for the remaining experiments. In Section 5.2, we present an offline-online training strategy for an optimal control problem whose initial conditions are not known in the training process of the SympNet. This experiment shows the generalizability of SympOCnet. Then, in Section 5.3, we demonstrate the performance of SympOCNet on a high-dimensional problem reported in [79]. From the results in Section 5.3, we observe that SympOCnet can handle the path planning problem whose state space has dimension 512, and hence the method can potentially mitigate the CoD. In Section 5.4, we apply SympOCnet to a swarm path planning problem in [74], and demonstrate good performance and efficiency in path planning problems, where the agents move in a three-dimensional space.

In Sections 5.1 and 5.2 we use a 6-layer SympNet with 60 hidden neurons in each layer and ReLU activation function. In Sections 5.3 and 5.4 we use a 6-layer SympNet with 200 hidden neurons in each layer and ReLU activation function. In all these experiments, the parameter λ in (3.6) is set to be 600, and the parameter $\tilde{\lambda}$ in (4.6) and (4.7) is set to be 200. By default, the time horizon T is set to be 1, and the speed limit C_v is 25. All the numerical experiments are run using a shared NVIDIA GeForce RTX 3090 GPU and a shared NVIDIA RTX A6000 GPU. In each experiment, we only show the figure for a part of the testing cases. More numerical results and codes are provided in <https://github.com/z Zhang222/SympOCNet>. Video animations of these examples are available online at https://github.com/z Zhang222/SympOCNet/tree/main/saved_results_animation.

5.1. Comparison among different loss functions. In this section, we consider the path planning problem with two obstacles and four drones in \mathbb{R}^2 . Each obstacle $E_j \subset \mathbb{R}^2$ is a convex set containing points whose distance to a line segment (denoted by $l_j \subset \mathbb{R}^2$) is less than a constant C_o . The initial positions of the four drones are $(-2, -2)$, $(2, -2)$, $(2, 2)$, $(-2, 2)$, and their terminal positions are $(2, 2)$, $(-2, 2)$, $(-2, -2)$, $(2, -2)$. Therefore, the optimal control problem (4.1) is an 8-dimensional problem, whose initial state \mathbf{x}_0 is $(-2, -2, 2, -2, 2, 2, -2, 2)$ and terminal state \mathbf{x}_T is $(2, 2, -2, 2, -2, -2, 2, -2)$. The obstacles and the initial positions of the four drones are shown in Figure 2.

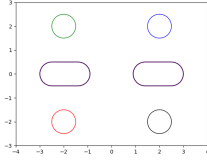


Fig. 2: **Initial positions of drones and obstacles.** The four drones located at their initial positions are represented by the four colored circles. The two obstacles are represented by round cornered rectangles in the middle.

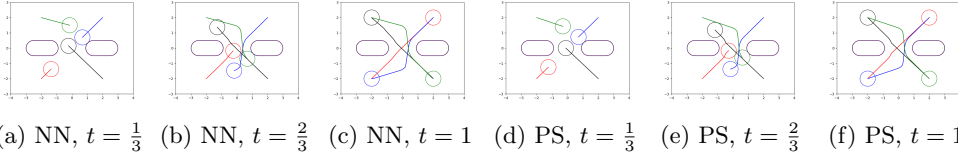


Fig. 3: **Output trajectories with loss \mathcal{L}_{aug} and pseudospectral method.** The left three figures show the trajectories of our proposed SympOCnet method at different time $t = \frac{1}{3}, \frac{2}{3}, 1$, and the right three figures show the outputs of the post-process (pseudospectral method) at different time $t = \frac{1}{3}, \frac{2}{3}, 1$. In each figure, the four colored circles show the positions of the four drones at time t , and the curves connected to the circles show the trajectories before time t .

To avoid the collisions of drones with obstacles, we define the first part of the constraint function h by (5.1), where each component d_j of the function d in (5.2) is defined by

$$d_j(\mathbf{x}) = \min_{\mathbf{y} \in l_j} \|\mathbf{x} - \mathbf{y}\|^2 - (C_o + C_d)^2 \quad \forall \mathbf{x} \in \mathbb{R}^2.$$

The term $\min_{\mathbf{y} \in l_j} \|\mathbf{x} - \mathbf{y}\|^2$ in d_j gives the squared distance between \mathbf{x} and the line segment l_j . Here, we use the squared distance instead of distance function to improve the smoothness of the constraint function h . Since the obstacle E_j contains all points whose distance to the line segment l_j is less than C_o , a drone collide with E_j if and only if the distance between its center and the line segment l_j is less than $C_o + C_d$. Therefore, such defined function d_j provides a constraint which avoids the collisions of drones with the j -th obstacle E_j .

Under this problem setup, we compare four different loss functions, i.e., the function \mathcal{L} defined in (3.6), \mathcal{L}_{log} in (4.6), \mathcal{L}_{quad} in (4.7), and \mathcal{L}_{aug} in (4.8). With each loss function, we train the neural network for 100,000 iterations, and then run the pseudospectral method to improve the results. By comparing the performance of the four loss functions in this example, we choose a better loss function for the other experiments in the remainder of this paper.

The outputs of the four loss functions are shown in Table 1, where the hyper-parameters in the penalty term $\epsilon\beta_a(h(\mathbf{x}(s)))$ are set to be $a = 0.004$ and $\epsilon = 0.0004$. Results for different loss functions are shown in different columns. For each loss function, we repeat the experiment 10 times with different random seeds, and then take

average to obtain the statistics in the table. We observe the convergence of the pseudospectral method in all repeated experiments, which shows the robustness of our SympOCnet method, providing optimal or suboptimal solutions in this example. The second to fourth lines in Table 1 show the minimal constraint value, the cost value in the optimal control problem, and the running time of the training process of our proposed SympOCnet method. The last four lines in Table 1 show the minimal constraint value, the cost value in the optimal control problem, the number of iterations, and the running time of the post-process using pseudospectral method.

loss function		\mathcal{L}	\mathcal{L}_{log}	\mathcal{L}_{quad}	\mathcal{L}_{aug}
SympOCnet	min constraint	-0.834	-0.00704	-0.0824	-4.84E-04
	cost	79.62	94.15	76.50	93.98
	running time (s)	1229	1776	1361	1708
PS	min constraint	-4.70E-09	-9.87E-12	-2.04E-12	-8.02E-13
	cost	73.47	91.00	76.95	80.91
	# iterations	49	19	17	23
	running time (s)	104	44	38	47

Table 1: **The comparison among results of four loss functions with SympOCnet method and pseudospectral post-process.** We show the minimal constraint value $\min_s h(\mathbf{x}(s))$, the cost $\int_{s=0}^T \frac{\|\mathbf{v}(s)\|^2}{2} ds$, and the running time of the SympOCnet as well as those statistics after the post-process. The loss function \mathcal{L}_{aug} provides the solution with least amount of constraint violations and reasonable cost values. It can be seen that in all cases, the SympOCnet provides a good initialization for the pseudospectral method.

minimal constraint	cost	number of iterations	running time (s)
-1.00E+00	64.00	5	44

Table 2: **The result of the pseudospectral method with the linear initialization.** We show the minimal constraint value $\min_s h(\mathbf{x}(s))$, the cost $\int_{s=0}^T \frac{\|\mathbf{v}(s)\|^2}{2} ds$, the number of iterations, and the running time of the pseudospectral method with the linear initialization (i.e., the initial trajectory is an affine function of the time variable, and the initial velocity is a constant function). The minimal constraint value is -1.00 , which shows that the constraint is not satisfied, and the pseudospectral method with the linear initialization does not converge to a feasible solution.

Comparing the results of the four loss functions, we observe that the penalty term and the augmented Lagrangian term in the loss function indeed improve the feasibility of the obtained trajectory. The constraints are better satisfied using the loss \mathcal{L}_{aug} in (4.8), while the corresponding cost value may be a little bit higher than the the results of \mathcal{L}_{quad} . In the other experiments, the problems are more complicated, and the constraints are harder to satisfy. Therefore, we use the loss function \mathcal{L}_{aug} for the experiments in the remainder of the paper to help enforce the state constraints. For simpler problems, other loss function may be more preferable for faster running time. How to choose the loss function adaptively may be a possible future direction.

Although the augmented Lagrangian method and log penalty loss function are slightly slower than the other two loss functions, it takes less than 30 minutes to run 100,000 training iterations, which shows the efficiency of SympOCnet.

To show the improvement using our proposed SympOCnet method as an initialization of the pseudospectral method, we solve the same problem using the pseudospectral method with the linear initialization, i.e., we set the initial guess of the pseudospectral method to be $\mathbf{v}(t) = \frac{\mathbf{x}_T - \mathbf{x}_0}{T}$ and $\mathbf{x}(t) = \frac{(\mathbf{x}_T - \mathbf{x}_0)t}{T}$ for any $t \in [0, T]$. The minimal constraint value, the cost value in the optimal control problem, the number of iterations, and the running time are shown in Table 2. The minimal constraint value in Table 2 is -1.00 , which shows that the pseudospectral method with the linear initialization does not converge to a feasible solution. Therefore, compared with the linear initialization, our SympOCnet method, no matter which loss function in \mathcal{L} , \mathcal{L}_{log} , \mathcal{L}_{quad} , and \mathcal{L}_{aug} we choose, provides a better initial guess for the pseudospectral method.

Moreover, we show the obtained results in one trial using SympOCnet with loss \mathcal{L}_{aug} and the post-process using the pseudospectral method in Figure 3. The left three figures show the trajectories of our proposed SympOCnet method at different times, while the right three figures correspond to the final results from the pseudospectral method at different times. In each figure, the four colored circles show the positions of the four drones at the specific time, and the curves connected to the circles show the trajectories before the current time. We observe that the shape of the trajectory given by our SympOCnet method does not change too much after the post-process, which shows that SympOCnet provides a suboptimal solution to the optimal control problem in this example.

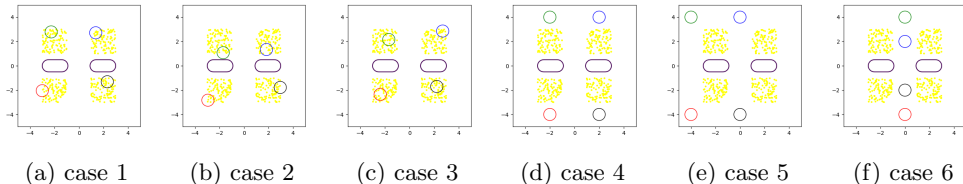


Fig. 4: **Initial positions of drones, obstacles, and training data.** In the six figures, we show the initial positions of the four drones (represented by colored circles), the positions of the two obstacles (represented by the round cornered rectangles), and the randomly sampled training data (represented by the yellow dots) in the six testing cases in Section 5.2.

5.2. Generalizability and offline-online training. In this section, we consider the same problem setup as in Section 5.1. To test the generalizability of SympOCnet, we assume that the exact initial position is unknown in the training process. We train one SympNet φ using multiple initial positions sampled from a uniform distribution centered at the initial position in Section 5.1. With multiple initial positions, we train one SympNet φ and several variables $\{(\mathbf{y}_{0k}, \mathbf{u}_k, \mathbf{q}_{0k})\}_k$, where the k -th trainable tuple $(\mathbf{y}_{0k}, \mathbf{u}_k, \mathbf{q}_{0k})$ corresponds to the k -th sampled initial position. We refer to this training process of the SympNet and all trainable variables as “offline training”. After 100,000 steps of offline training, the exact initial positions are provided. To

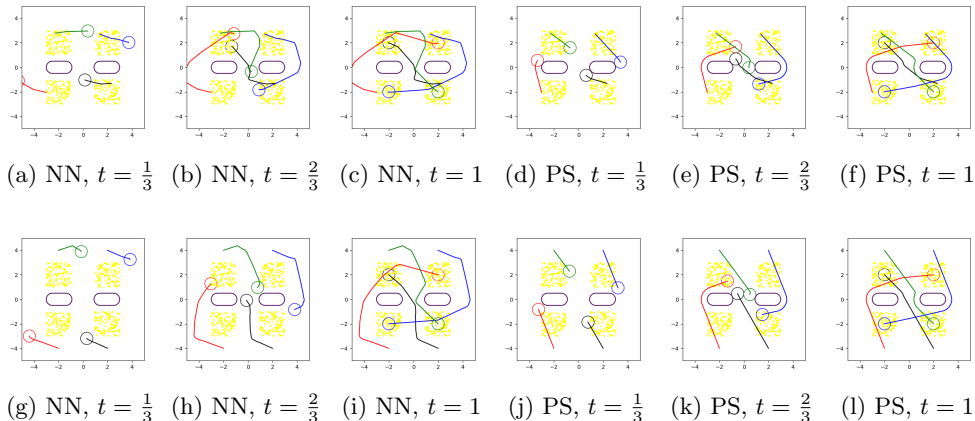


Fig. 5: **Output trajectories of offline-online training and post-process.** The first and second rows correspond to the first and fourth case, respectively. The left three columns are the output from L-BFGS, and the right three columns are the output from the pseudospectral method. In each figure, the four colored circles show the positions of the four drones at time t , and the curves connected to the circles show the trajectories before time t .

obtain an improved solution in reasonable running time using the trained SympNet φ as well as the new information, we fix the SympNet φ and apply the L-BFGS method to train the variables $(\mathbf{y}_0, \mathbf{u}, \mathbf{q}_0)$ with the exact initial and terminal positions. We call this training process using L-BFGS method the “online training”. The optimal trajectory is then computed using (3.7), where φ_1 comes from the SympNet φ trained in the offline training, and the parameters $(\mathbf{y}_0, \mathbf{u}, \mathbf{q}_0)$ are outputted from the online training. After the online training, we also apply the pseudospectral method to improve the quality of the results.

To generate training data for the initial positions, we sample 100 points from the uniform distribution in $[x - 1, x + 1] \times [y - 1, y + 1]$ where (x, y) is the initial position of a drone in Section 5.1. To test the generalizability of our method, we have six cases. In the first three cases, the exact initial positions are randomly sampled from the same distribution used to generate the training data. In other words, we assume the exact data is covered in the area of the training data. In the last three cases, we set the initial conditions for the state variable to be $(-2, -4, 2, -4, 2, 4, -2, 4)$, $(-4, -4, 0, -4, 0, 4, -4, 4)$, and $(0, -4, 0, -2, 0, 2, 0, 4)$, respectively. These three initial positions are not in the range of the training data. Therefore, the results with these three initial positions show the generalizability of our SympOCnet method when the test data is not covered by the area of the training data. The initial positions of the drones, the positions of the obstacles, and the training data are shown in Figure 4, where the four colored circles denote the drones, the two round cornered rectangles denote the obstacles, and the yellow dots denote the sampled training data.

In our experiments, we found that the performance is improved if we increase the dimension of the problem by adding some latent variables. We increase the dimension

of the state space from 8 to 16, and define the Hamiltonian on the larger space by

$$H(\mathbf{x}_1, \mathbf{x}_2, \mathbf{p}_1, \mathbf{p}_2) = H_{\epsilon, a}(\mathbf{x}_1, \mathbf{p}_1) + \frac{1}{2} \|\mathbf{p}_2\|^2 \quad \forall \mathbf{x}_1, \mathbf{x}_2, \mathbf{p}_1, \mathbf{p}_2 \in \mathbb{R}^8,$$

where $(\mathbf{x}_1, \mathbf{p}_1)$ are the variables in the original problem, $(\mathbf{x}_2, \mathbf{p}_2)$ are the latent variables we add, and $H_{\epsilon, a}$ is the function defined in (4.5). The minimal constraint, cost in the optimal control problem, and running time of the L-BFGS method and pseudospectral method are shown in Table 3. As in Section 5.1, we run 10 repeated experiments and put their average values in the table. In the online training, we run 1,000 L-BFGS iterations to train the parameters of all the six cases simultaneously. Note that we can train them all at once, since they share the same SympNet, and the loss function is the summation of the loss functions in all cases. Then, we run the pseudospectral method on each case until it converges. The statistics for the L-BFGS training and the pseudospectral method for the six cases are shown in each line of Table 3. The minimal constraint value of L-BFGS method is not as good as the results in Section 5.1, which is expected, since the initial positions are not known when the SympNet is trained. However, from the minimal constraint values of the pseudospectral post-process in the six cases, we conclude that our offline-online training still provides a good initialization for the pseudospectral method, which shows a good generalizability of our proposed method.

	minimal constraint	cost	time (s)
L-BFGS	-1.27E-04	231.44	158
PS (case 1)	-1.97E-11	102.00	59
PS (case 2)	-1.74E-11	94.59	77
PS (case 3)	-3.36E-11	90.95	79
PS (case 4)	-6.00E-09	141.22	65
PS (case 5)	-7.19E-08	140.47	111
PS (case 6)	1.64E-13	112.41	67

Table 3: **The results given by the offline-online training (L-BFGS) and the post-process (pseudospectral method) in six generalizability tests.** The offline-online training using L-BFGS method provides a good initialization for the pseudospectral method. With this initialization, the pseudospectral method in the post-process improves the feasibility and optimality of the solution in all the six cases.

We also compare our results with the pseudospectral method whose initialization is given by the linear interpolation (as described in Section 5.1) in the six generalizability tests. The minimal constraint value, cost value in the optimal control problem, and running time of the pseudospectral method with the linear initialization are shown in Table 4. Comparing Table 3 with Table 4, we see that although our proposed method has slightly larger cost values in the first five cases, the pseudospectral method with the linear initialization does not converge to a feasible solution in the last case. Therefore, our proposed method provides a more robust initialization for the pseudospectral method compared with the linear initialization.

Moreover, we plot the output trajectories of one trial of the first and fourth cases computed using our proposed method in Figure 5. The left three columns show the output trajectory given by the offline-online training, and the right three columns are the output trajectory from the post-process. In each figure, the yellow dots are the

	minimal constraint	cost	time (s)
PS (linear initialization, case 1)	-7.71E-09	85.19	134
PS (linear initialization, case 2)	2.95E-07	83.98	173
PS (linear initialization, case 3)	-1.94E-10	79.67	178
PS (linear initialization, case 4)	-5.55E-16	80.44	157
PS (linear initialization, case 5)	-8.08E-14	136.16	147
PS (linear initialization, case 6)	-1.00	60.00	28

Table 4: **The results given by the pseudospectral method with the linear initialization in six generalizability tests.** Although the pseudospectral method with the linear initialization performs slightly better than our proposed method in the first five cases, it violates the constraint in the last case. Therefore, our proposed method provides a more robust initialization for the pseudospectral method compared with the linear initialization.

initial positions of the sampled training data. Similar as in Section 5.1, the four colored circles show the current positions of the four drones, and the curves connected to them illustrate the trajectories before the current time. The first row in Figure 5 is for the first case where the exact initial positions are in the area of the sampled training data. The second row is for the fourth case where the exact initial positions are outside the area of the training data. We observe that the offline-online training process still provides feasible trajectories in both cases, based on which the post-process improves the smoothness of the trajectories to provide more optimal solutions. Therefore, our proposed SympOCnet method has the generalizability to handle unseen data which are close to the training data.

5.3. Multiple drones in a two-dimensional room. In this section, we consider the path planning problem for multiple drones in a room, which is inspired by [79]. To be specific, we consider M drones moving in a room $[-C_r, C_r]^2$ for some $C_r > 0$. In our experiments, we set the constant $C_r = 5$ (i.e., the room has size 10×10). We need to avoid the collisions among the drones as well as the collisions between drones and the walls. The constraint function $h = (h_1, h_2)$ contains two parts: the function h_2 is defined by (5.3), and the function h_1 is the obstacle constraint provided by the four walls. Hence, we set h_1 in the form of (5.1), where the function d is defined by $d(\mathbf{x}) = (x_1 + C_r, C_r - x_1, x_2 + C_r, C_r - x_2)$ for any $\mathbf{x} = (x_1, x_2) \in \mathbb{R}^2$. The initial positions of the drones are near the boundary of the room, and the terminal positions are the opposite locations, i.e., we set $\mathbf{x}_T = -\mathbf{x}_0$. This is a high-dimensional example (the dimension of the state space is $n = 2M$, which ranges from 64 to 512 in our experiments), and hence we apply our SympOCnet method without the post-process.

First, we set the drone radius C_d to be 0.3. We run 10 repeated experiments (with 100,000 training iterations in each experiment) with drone numbers $M = 32$ and 64 to test the robustness of our SympOCnet method. The results are shown in Table 5. In each trial, we compute the minimal normalized distance of any pair of drones at any time grid, i.e., we compute \mathcal{D} defined by

$$\mathcal{D} = \frac{1}{2C_d} \min_{1 \leq i < j \leq M} \min_{1 \leq k \leq N} \|\mathbf{x}_i(t_k) - \mathbf{x}_j(t_k)\|,$$

where $\mathbf{x}_i(t_k)$ denotes the center position for the i -th drone at time t_k . Then, we

compute the average and standard deviation of these minimal normalized distances \mathcal{D} in the 10 trials, which are shown in the second and third columns in Table 5. We also compute the scaled cost in the optimal control problem, which is defined by $\frac{1}{M} \int_0^T \frac{1}{2} \|\dot{\mathbf{x}}(t)\|^2 dt$, where $\mathbf{x}(\cdot)$ is the output trajectory for the state variable \mathbf{x} in the optimal control problem. The average of the scaled cost is shown in the fourth column in Table 5. In the last column of Table 5, we show the averaged running time of the training process. From the results, we observe that our SympOCnet method provides feasible results in reasonable running time for this high-dimensional problem. Note that the collision between two drones happens whenever the minimal normalized distance is less than 1. Therefore, in general the collision does not happen for 32 drones, but it may happen for 64 or more drones. To provide a more feasible solution, in the following experiments, we put a safe zone outside each drone by setting C_d to be a little bit larger than the actual drone radius.

# drones	$\mathbb{E}(\mathcal{D})$	$\text{std}(\mathcal{D})$	scaled cost	time (s)
32	1.001	0.00390	85.84	1905
64	0.986	0.00347	100.43	2214

Table 5: **The results for the path planning problem with 32 and 64 drones in a room.** We show the expected value and standard deviation of the minimal normalized distances. The collision does not happen for 32 drones, but it may happen for 64 or more drones. Therefore, we need to put a safe zone near each drone to avoid collision when the number of drones is large. The computation time increases only by 309 seconds when scaling from 32 to 64 drones.

We also tested our SympOCnet method on this path planning problem with 128 drones (whose radius is 0.075) and four obstacles. The initial and terminal positions are similar to the cases of 32 or 64 drones (see Figure 6 (a) and (d)). The four obstacles are balls inside the room, which are represented by the black circles in Figure 6. The constraint function d_j in (5.2) corresponding to the obstacle E_j is defined by $d_j(\mathbf{x}) = \|\mathbf{z}_j - \mathbf{x}\|^2 - (C_o + C_d)^2$ for any $\mathbf{x} \in \mathbb{R}^n$, where $\mathbf{z}_j \in \mathbb{R}^2$ and $C_o > 0$ are the center and radius of the obstacle E_j , respectively. The results are shown in Figure 6. Each figure shows the current positions (represented by colored circles) and the previous trajectories (represented by grey curves) of the drones at different time $t = 0, \frac{1}{3}, \frac{2}{3}, 1$. To provide a feasible solution, we set C_d in the constraint function to be 0.1 instead of 0.075. It takes 4161 seconds to finish 100,000 training iterations. From the numerical results, we found that there are no collisions between obstacles and drones, and hence SympOCnet performs well and efficiently in this high-dimensional problem.

Then, we tested our proposed method on a higher dimensional problem. We set the drone number $M = 256$, and hence the dimension of the state space is $n = 2M = 512$. We solve this path planning problem with 256 drones (whose radius is 0.09) in the two-dimensional room $[-5, 5]^2$. The initial positions are shown in Figure 7 (a), and the terminal condition is $\mathbf{x}_T = -\mathbf{x}_0$. The results are shown in Figure 7. To provide a feasible solution, we add a safe zone and set C_d in the state constraint to be 0.1 instead of 0.09. From this result, we observe no collisions among the drones. It takes 5481 seconds to obtain this feasible solution in 100,000 training iterations. Therefore, SympOCnet is able to efficiently solve this 512-dimensional path planning problem.

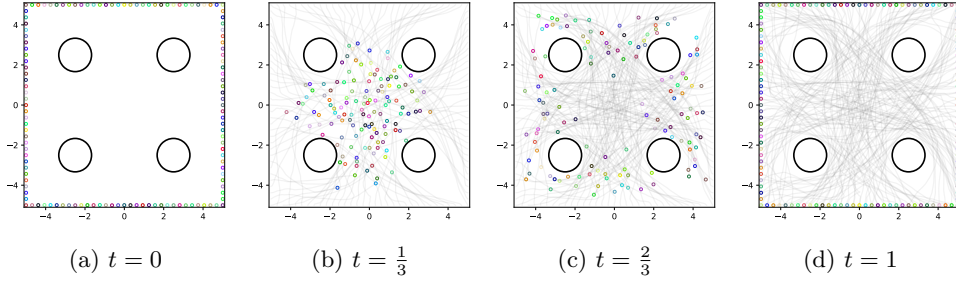


Fig. 6: **Path planning of 128 drones with four obstacles on the plane.** We plot the predicted positions of 128 drones at time $t = 0, \frac{1}{3}, \frac{2}{3}, 1$. The four black circles represent the four obstacles, and the colored circles represent the drones. The paths from the initial conditions to the current positions of all drones are plotted as gray lines. There are no collisions in the three clipped snapshots, and the planned trajectories are all inside the 10×10 square.

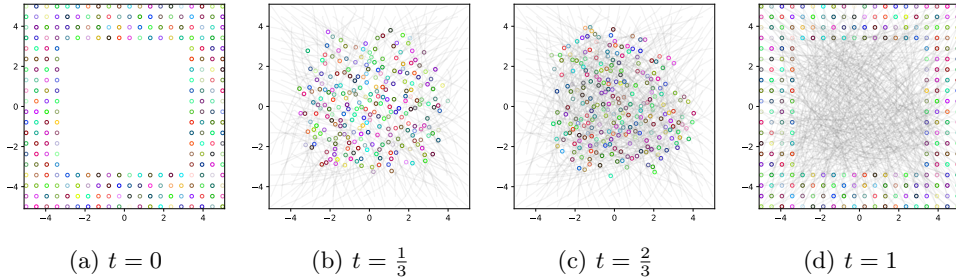


Fig. 7: **Path planning of 256 drones on the plane.** We plot the predicted positions of 256 drones at time $t = 0, \frac{1}{3}, \frac{2}{3}, 1$. The drones are represented by colored circles. The paths from the initial positions to the current positions of all drones are plotted as gray lines. There are no collisions in the three clipped snapshots, and the planned trajectories are inside the 10×10 square.

5.4. Multiple drones with obstacle avoidance in a three-dimensional space. We consider the three-dimensional swarm path planning example in [74]. To be specific, we consider $M = 100$ drones with radius 0.18. Their goal is to avoid two obstacles which are located between their initial positions and terminal positions, as illustrated in Figure 8. The total dimension of the state space is $n = 3M = 300$. The j -th obstacle E_j is defined to be the rectangular set $[C_{11}^j, C_{12}^j] \times [C_{21}^j, C_{22}^j] \times [C_{31}^j, C_{32}^j]$, where C_{ik}^j is a constant scalar. We set the constraint function $h = (h_1, h_2)$ in the same way as described before, where the function d_j in (5.2) is defined by

$$d_j(\mathbf{x}) = \max\{C_{i1}^j - C_d - x_i, x_i - C_{i2}^j - C_d : i = 1, 2, 3\},$$

for each $j = 1, 2$ and $\mathbf{x} = (x_1, x_2, x_3) \in \mathbb{R}^3$. Note that $d_j(\mathbf{x}) \leq 0$ if and only if $x_i \in [C_{i1}^j - C_d, C_{i2}^j + C_d]$ for each $i = 1, 2, 3$, which holds if the ball centered at \mathbf{x} with radius C_d intersects with the obstacle E_j . Therefore, the constraint $d_j(\mathbf{x}) \geq 0$

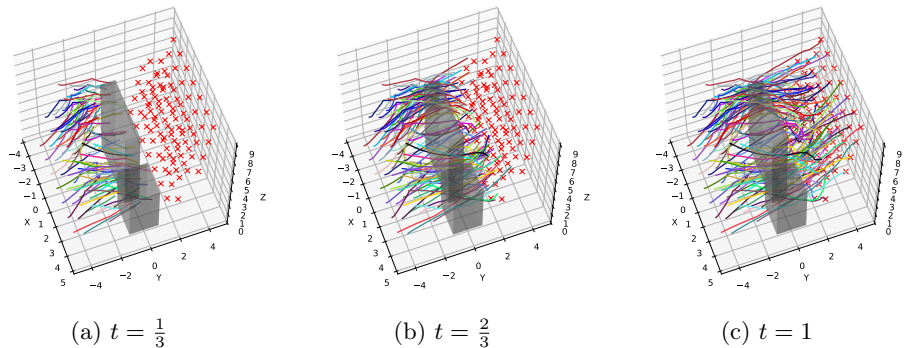


Fig. 8: **Path planning of 100 drones in a 3d space.** We plot the predicted positions of 100 drones at time $t = \frac{1}{3}, \frac{2}{3}, 1$. The paths from the initial positions to the current positions of all drones are plotted as colored lines. The destinations are marked as red crosses. The drones reach their destinations without any collision.

enforces the drones to avoid collisions with the obstacle E_j . In our experiment, we set

$$\begin{aligned} (C_{11}^1, C_{12}^1, C_{21}^1, C_{22}^1, C_{31}^1, C_{32}^1) &= (-1.8, 1.8, -0.3, 0.3, 0.2, 6.8), \\ (C_{11}^2, C_{12}^2, C_{21}^2, C_{22}^2, C_{31}^2, C_{32}^2) &= (2.2, 3.8, -0.8, 0.8, 0.2, 3.8). \end{aligned}$$

In other words, the constraint sets are $[-1.8, 1.8] \times [-0.3, 0.3] \times [0.2, 6.8]$ and $[2.2, 3.8] \times [-0.8, 0.8] \times [0.2, 3.8]$. We apply our proposed SympOCnet method to solve this 300-dimensional problem, and plot the result in Figure 8. Due to the high dimensionality, we do not apply the post-process. To provide a feasible solution, we set C_d in the state constraint to be 0.2 instead of 0.18. From the numerical results, we observe no collisions among the drones and the obstacles. The minimal distance between every pair of drones is 0.3994, which is bigger than twice of the radius. It takes 3633 seconds to finish 150,000 training iterations. Therefore, our proposed SympOCnet method provides a feasible solution to this high-dimensional swarm path planning problem in reasonable time.

6. Summary. We have proposed a novel SympOCnet method for efficiently solving high-dimensional optimal control problems with state constraints. We applied SympOCnet to several multi-agent simultaneous path planning problems with obstacle avoidance. The numerical results show SympOCnet’s ability to solve high-dimensional problems efficiently with dimension more than 500. These first results reveal the potential of SympOCnet for solving high-dimensional optimal control problems in real-time. In future work, we are going to consider possible combinations with the DeepONet architecture [64] to avoid any training cost during inference and to endow the predictive system with uncertainties, such as uncertain initial and terminal positions in path planning problems.

Acknowledgement. The simulations were run on GeForce RTX 3090 and RTX A6000 GPU donated to us by NVIDIA.

REFERENCES

- [1] M. AKIAN, R. BAPAT, AND S. GAUBERT, *Max-plus algebra*, Handbook of linear algebra, 39 (2006).
- [2] M. AKIAN, S. GAUBERT, AND A. LAKHOVA, *The max-plus finite element method for solving deterministic optimal control problems: basic properties and convergence analysis*, SIAM Journal on Control and Optimization, 47 (2008), pp. 817–848.
- [3] A. ALLA, M. FALCONE, AND L. SALUZZI, *An efficient DP algorithm on a tree-structure for finite horizon optimal control problems*, SIAM Journal on Scientific Computing, 41 (2019), pp. A2384–A2406.
- [4] A. ALLA, M. FALCONE, AND S. VOLKWEIN, *Error analysis for POD approximations of infinite horizon problems via the dynamic programming approach*, SIAM Journal on Control and Optimization, 55 (2017), pp. 3091–3115.
- [5] A. BACHOUCH, C. HURÉ, N. LANGRENÉ, AND H. PHAM, *Deep neural networks algorithms for stochastic control problems on finite horizon: numerical applications*, arXiv preprint arXiv:1812.05916, (2018).
- [6] S. BANSAL AND C. J. TOMLIN, *Deepreach: A deep learning approach to high-dimensional reachability*, in 2021 IEEE International Conference on Robotics and Automation (ICRA), IEEE, 2021, pp. 1817–1824.
- [7] R. E. BELLMAN, *Adaptive control processes: a guided tour*, Princeton university press, 1961.
- [8] D. P. BERTSEKAS, *Reinforcement learning and optimal control*, Athena Scientific, Belmont, Massachusetts, (2019).
- [9] O. BOKANOWSKI, N. GAMMOUDI, AND H. ZIDANI, *Optimistic Planning Algorithms For State-Constrained Optimal Control Problems*. working paper or preprint, July 2021, <https://hal.archives-ouvertes.fr/hal-03283075>.
- [10] O. BOKANOWSKI, J. GARCKE, M. GRIEBEL, AND I. KLOMPMAKER, *An adaptive sparse grid semi-Lagrangian scheme for first order Hamilton-Jacobi Bellman equations*, Journal of Scientific Computing, 55 (2013), pp. 575–605.
- [11] M. CHEN, J. F. FISAC, S. SASTRY, AND C. J. TOMLIN, *Safe sequential path planning of multi-vehicle systems via double-obstacle Hamilton-Jacobi-Isaacs variational inequality*, in 2015 European Control Conference (ECC), IEEE, 2015, pp. 3304–3309.
- [12] M. CHEN, Q. HU, J. F. FISAC, K. AKAMETALU, C. MACKIN, AND C. J. TOMLIN, *Reachability-based safety and goal satisfaction of unmanned aerial platoons on air highways*, Journal of Guidance, Control, and Dynamics, 40 (2017), pp. 1360–1373.
- [13] M. CHEN AND C. J. TOMLIN, *Exact and efficient Hamilton-Jacobi reachability for decoupled systems*, in 2015 54th IEEE Conference on Decision and Control (CDC), IEEE, 2015, pp. 1297–1303.
- [14] P. CHEN, J. DARBON, AND T. MENG, *Hopf-type representation formulas and efficient algorithms for certain high-dimensional optimal control problems*, arXiv preprint arXiv:2110.02541, (2021).
- [15] P. CHEN, J. DARBON, AND T. MENG, *Lax-Oleinik-type formulas and efficient algorithms for certain high-dimensional optimal control problems*, arXiv preprint arXiv:2109.14849, (2021).
- [16] A. R. CONN, N. I. GOULD, AND P. TOINT, *A globally convergent augmented Lagrangian algorithm for optimization with general constraints and simple bounds*, SIAM Journal on Numerical Analysis, 28 (1991), pp. 545–572.
- [17] M. COUPECHOUX, J. DARBON, J.-M. KÉLIF, AND M. SIGELLE, *Optimal trajectories of a UAV base station using Lagrangian mechanics*, in IEEE INFOCOM 2019-IEEE Conference on Computer Communications Workshops (INFOCOM WKSHPS), IEEE, 2019, pp. 626–631.
- [18] J. DARBON, *On convex finite-dimensional variational methods in imaging sciences and Hamilton-Jacobi equations*, SIAM Journal on Imaging Sciences, 8 (2015), pp. 2268–2293, <https://doi.org/10.1137/130944163>, <https://arxiv.org/abs/https://doi.org/10.1137/130944163>.
- [19] J. DARBON, P. M. DOWER, AND T. MENG, *Neural network architectures using min plus algebra for solving certain high dimensional optimal control problems and Hamilton-Jacobi PDEs*, arXiv preprint arXiv:2105.03336, (2021).
- [20] J. DARBON, G. P. LANGLOIS, AND T. MENG, *Overcoming the curse of dimensionality for some Hamilton-Jacobi partial differential equations via neural network architectures*, Res. Math. Sci., 7 (2020), p. 20, <https://doi.org/10.1007/s40687-020-00215-6>, <https://doi.org/10.1007/s40687-020-00215-6>.
- [21] J. DARBON AND T. MENG, *On decomposition models in imaging sciences and multi-time Hamilton-Jacobi partial differential equations*, SIAM Journal on Imaging Sciences, 13 (2020), pp. 971–1014, <https://doi.org/10.1137/19M1266332>, <https://doi.org/10.1137/19M1266332>.

- 19M1266332, <https://arxiv.org/abs/https://doi.org/10.1137/19M1266332>.
- [22] J. DARBON AND T. MENG, *On some neural network architectures that can represent viscosity solutions of certain high dimensional Hamilton–Jacobi partial differential equations*, Journal of Computational Physics, 425 (2021), p. 109907, <https://doi.org/https://doi.org/10.1016/j.jcp.2020.109907>, <http://www.sciencedirect.com/science/article/pii/S0021999120306811>.
- [23] J. DARBON, T. MENG, AND E. RESMERITA, *On Hamilton–Jacobi PDEs and image denoising models with certain non-additive noise*, arXiv preprint arXiv:2105.13997, (2021).
- [24] J. DARBON AND S. OSHER, *Algorithms for overcoming the curse of dimensionality for certain Hamilton–Jacobi equations arising in control theory and elsewhere*, Res Math Sci Research in the Mathematical Sciences, 3 (2016), pp. 1–26, <https://doi.org/10.1186/s40687-016-0068-7>, <https://doi.org/10.1186/s40687-016-0068-7>.
- [25] D. DELAHAYE, S. PUECHMOREL, P. TSOTRAS, AND E. FÉRON, *Mathematical models for aircraft trajectory design: A survey*, in Air Traffic Management and Systems, Springer, 2014, pp. 205–247.
- [26] J. DENK AND G. SCHMIDT, *Synthesis of a walking primitive database for a humanoid robot using optimal control techniques*, in Proceedings of IEEE-RAS International Conference on Humanoid Robots, 2001, pp. 319–326.
- [27] B. DJERIDANE AND J. LYGEROS, *Neural approximation of PDE solutions: An application to reachability computations*, in Proceedings of the 45th IEEE Conference on Decision and Control, Dec 2006, pp. 3034–3039, <https://doi.org/10.1109/CDC.2006.377184>.
- [28] S. DOLGOV, D. KALISE, AND K. K. KUNISCH, *Tensor decomposition methods for high-dimensional Hamilton–Jacobi–Bellman equations*, SIAM Journal on Scientific Computing, 43 (2021), pp. A1625–A1650, <https://doi.org/10.1137/19M1305136>, <https://doi.org/10.1137/19M1305136>, <https://arxiv.org/abs/https://doi.org/10.1137/19M1305136>.
- [29] P. M. DOWER, W. M. MCEANEY, AND H. ZHANG, *Max-plus fundamental solution semigroups for optimal control problems*, in 2015 Proceedings of the Conference on Control and its Applications, SIAM, 2015, pp. 368–375.
- [30] A. EL KHOURY, F. LAMIRAUX, AND M. TAIX, *Optimal motion planning for humanoid robots*, in 2013 IEEE International Conference on Robotics and Automation, IEEE, 2013, pp. 3136–3141.
- [31] F. FAHROO AND I. M. ROSS, *Costate estimation by a Legendre pseudospectral method*, Journal of Guidance, Control, and Dynamics, 24 (2001), pp. 270–277.
- [32] F. FAHROO AND I. M. ROSS, *Direct trajectory optimization by a Chebyshev pseudospectral method*, Journal of Guidance, Control, and Dynamics, 25 (2002), pp. 160–166.
- [33] M. FALLON, S. KUINDERSMA, S. KARUMANCHI, M. ANTONE, T. SCHNEIDER, H. DAI, C. P. D’ARPINO, R. DEITS, M. DICICCO, D. FOURIE, T. KOOLEN, P. MARION, M. POSA, A. VALENZUELA, K.-T. YU, J. SHAH, K. IAGNEMMA, R. TEDRAKE, AND S. TELLER, *An architecture for online affordance-based perception and whole-body planning*, Journal of Field Robotics, 32 (2015), pp. 229–254.
- [34] S. FENG, E. WHITMAN, X. XINJILEFU, AND C. G. ATKESON, *Optimization based full body control for the atlas robot*, in 2014 IEEE-RAS International Conference on Humanoid Robots, IEEE, 2014, pp. 120–127.
- [35] W. FLEMING AND W. MCEANEY, *A max-plus-based algorithm for a Hamilton–Jacobi–Bellman equation of nonlinear filtering*, SIAM Journal on Control and Optimization, 38 (2000), pp. 683–710, <https://doi.org/10.1137/S0363012998332433>.
- [36] K. FUJIWARA, S. KAJITA, K. HARADA, K. KANEKO, M. MORISAWA, F. KANEHIRO, S. NAKAOKA, AND H. HIRUKAWA, *An optimal planning of falling motions of a humanoid robot*, in 2007 IEEE/RSJ International Conference on Intelligent Robots and Systems, IEEE, 2007, pp. 456–462.
- [37] J. GARCKE AND A. KRÖNER, *Suboptimal feedback control of PDEs by solving HJB equations on adaptive sparse grids*, Journal of Scientific Computing, 70 (2017), pp. 1–28.
- [38] D. GARG, *Advances in global pseudospectral methods for optimal control*, PhD thesis, University of Florida Gainesville, FL, 2011.
- [39] S. GAUBERT, W. MCEANEY, AND Z. QU, *Curse of dimensionality reduction in max-plus based approximation methods: Theoretical estimates and improved pruning algorithms*, in 2011 50th IEEE Conference on Decision and Control and European Control Conference, IEEE, 2011, pp. 1054–1061.
- [40] S. GREYDANUS, M. DZAMBA, AND J. YOSINSKI, *Hamiltonian neural networks*, in Advances in Neural Information Processing Systems, H. Wallach, H. Larochelle, A. Beygelzimer, F. d’Alché-Buc, E. Fox, and R. Garnett, eds., vol. 32, Curran Associates, Inc., 2019, <https://proceedings.neurips.cc/paper/2019/file/26cd8ecadce0d4efd6cc8a8725cbd1f8-Paper.pdf>.
- [41] E. HAIRER, M. HOCHBRUCK, A. ISERLES, AND C. LUBICH, *Geometric numerical integration*,

- Oberwolfach Reports, 3 (2006), pp. 805–882.
- [42] J. HAN, A. JENTZEN, AND W. E, *Solving high-dimensional partial differential equations using deep learning*, Proceedings of the National Academy of Sciences, 115 (2018), pp. 8505–8510, <https://doi.org/10.1073/pnas.1718942115>.
- [43] M. HOFER, M. MUEHLEBACH, AND R. D'ANDREA, *Application of an approximate model predictive control scheme on an unmanned aerial vehicle*, in 2016 IEEE International Conference on Robotics and Automation (ICRA), IEEE, 2016, pp. 2952–2957.
- [44] M. B. HOROWITZ, A. DAMLE, AND J. W. BURDICK, *Linear Hamilton Jacobi Bellman equations in high dimensions*, in 53rd IEEE Conference on Decision and Control, IEEE, 2014, pp. 5880–5887.
- [45] C. HURÉ, H. PHAM, A. BACHOUCH, AND N. LANGRENÉ, *Deep neural networks algorithms for stochastic control problems on finite horizon: Convergence analysis*, SIAM Journal on Numerical Analysis, 59 (2021), pp. 525–557, <https://doi.org/10.1137/20M1316640>, <https://doi.org/10.1137/20M1316640>, <https://arxiv.org/abs/https://doi.org/10.1137/20M1316640>.
- [46] C. HURÉ, H. PHAM, AND X. WARIN, *Some machine learning schemes for high-dimensional nonlinear PDEs*, arXiv preprint arXiv:1902.01599, (2019).
- [47] F. JIANG, G. CHOU, M. CHEN, AND C. J. TOMLIN, *Using neural networks to compute approximate and guaranteed feasible Hamilton-Jacobi-Bellman PDE solutions*, arXiv preprint arXiv:1611.03158, (2016).
- [48] L. JIN, S. LI, J. YU, AND J. HE, *Robot manipulator control using neural networks: A survey*, Neurocomputing, 285 (2018), pp. 23 – 34, <https://doi.org/https://doi.org/10.1016/j.neucom.2018.01.002>, <http://www.sciencedirect.com/science/article/pii/S0925231218300158>.
- [49] P. JIN, Z. ZHANG, I. G. KEVREKIDIS, AND G. E. KARNIADAKIS, *Learning Poisson systems and trajectories of autonomous systems via Poisson neural networks*, arXiv preprint arXiv:2012.03133, (2020).
- [50] P. JIN, Z. ZHANG, A. ZHU, Y. TANG, AND G. E. KARNIADAKIS, *SympNets: Intrinsic structure-preserving symplectic networks for identifying Hamiltonian systems*, Neural Networks, 132 (2020), pp. 166–179.
- [51] D. KALISE, S. KUNDU, AND K. KUNISCH, *Robust feedback control of nonlinear PDEs by numerical approximation of high-dimensional Hamilton-Jacobi-Isaacs equations*, arXiv preprint arXiv:1905.06276, (2019).
- [52] D. KALISE AND K. KUNISCH, *Polynomial approximation of high-dimensional Hamilton–Jacobi–Bellman equations and applications to feedback control of semilinear parabolic PDEs*, SIAM Journal on Scientific Computing, 40 (2018), pp. A629–A652.
- [53] W. KANG AND L. C. WILCOX, *Mitigating the curse of dimensionality: sparse grid characteristics method for optimal feedback control and HJB equations*, Computational Optimization and Applications, 68 (2017), pp. 289–315.
- [54] Y. H. KIM, F. L. LEWIS, AND D. M. DAWSON, *Intelligent optimal control of robotic manipulators using neural networks*, Automatica, 36 (2000), pp. 1355 – 1364, [https://doi.org/https://doi.org/10.1016/S0005-1098\(00\)00045-5](https://doi.org/https://doi.org/10.1016/S0005-1098(00)00045-5), <http://www.sciencedirect.com/science/article/pii/S0005109800000455>.
- [55] M. R. KIRCHNER, M. J. DEBORD, AND J. P. HESPANHA, *A Hamilton–Jacobi formulation for optimal coordination of heterogeneous multiple vehicle systems*, in 2020 IEEE/RSJ International Conference on Intelligent Robots and Systems (IROS), IEEE, 2020, pp. 11623–11630.
- [56] S. KUINDERSMA, R. DEITS, M. FALLON, A. VALENZUELA, H. DAI, F. PERMENTER, T. KOOLEN, P. MARION, AND R. TEDRAKE, *Optimization-based locomotion planning, estimation, and control design for the atlas humanoid robot*, Autonomous robots, 40 (2016), pp. 429–455.
- [57] K. KUNISCH, S. VOLKWEIN, AND L. XIE, *HJB-POD-based feedback design for the optimal control of evolution problems*, SIAM Journal on Applied Dynamical Systems, 3 (2004), pp. 701–722.
- [58] P. LAMBRIANIDES, Q. GONG, AND D. VENTURI, *A new scalable algorithm for computational optimal control under uncertainty*, Journal of Computational Physics, 420 (2020), p. 109710, <https://doi.org/https://doi.org/10.1016/j.jcp.2020.109710>, <https://www.sciencedirect.com/science/article/pii/S0021999120304848>.
- [59] D. LEE AND C. J. TOMLIN, *A Hopf-Lax formula in Hamilton–Jacobi analysis of reach-avoid problems*, IEEE Control Systems Letters, 5 (2020), pp. 1055–1060.
- [60] D. LEE AND C. J. TOMLIN, *A Computationally Efficient Hamilton-Jacobi-based Formula for State-Constrained Optimal Control Problems*, arXiv e-prints, (2021), arXiv:2106.13440, p. arXiv:2106.13440, <https://arxiv.org/abs/2106.13440>.
- [61] F. LEWIS, D. DAWSON, AND C. ABDALLAH, *Robot Manipulator Control: Theory and Prac-*

- tice, Control engineering, Marcel Dekker, 2004, <https://books.google.com/books?id=BDS.PQAACAAJ>.
- [62] A. LI, S. BANSAL, G. GIOVANIS, V. TOLANI, C. TOMLIN, AND M. CHEN, *Generating robust supervision for learning-based visual navigation using Hamilton-Jacobi reachability*, in Learning for Dynamics and Control, PMLR, 2020, pp. 500–510.
- [63] F. LIN AND R. D. BRANDT, *An optimal control approach to robust control of robot manipulators*, IEEE Transactions on robotics and automation, 14 (1998), pp. 69–77.
- [64] L. LU, P. JIN, G. PANG, Z. ZHANG, AND G. E. KARNIADAKIS, *Learning nonlinear operators via DeepONet based on the universal approximation theorem of operators*, Nature Machine Intelligence, 3 (2021), pp. 218–229.
- [65] V. R. MAKKAPATI, J. RIDDERHOF, P. TSIOTRAS, J. HART, AND B. VAN BLOEMEN WAANDERS, *Desensitized trajectory optimization for hypersonic vehicles*, in 2021 IEEE Aerospace Conference (50100), 2021, pp. 1–10, <https://doi.org/10.1109/AERO50100.2021.9438511>.
- [66] W. MCENEANEY, *A curse-of-dimensionality-free numerical method for solution of certain HJB PDEs*, SIAM Journal on Control and Optimization, 46 (2007), pp. 1239–1276, <https://doi.org/10.1137/040610830>.
- [67] W. M. MCENEANEY, *Max-plus methods for nonlinear control and estimation*, Systems & Control: Foundations & Applications, Birkhäuser Boston, Inc., Boston, MA, 2006.
- [68] W. M. MCENEANEY, A. DESHPANDE, AND S. GAUBERT, *Curse-of-complexity attenuation in the curse-of-dimensionality-free method for HJB PDEs*, in 2008 American Control Conference, IEEE, 2008, pp. 4684–4690.
- [69] W. M. MCENEANEY AND L. J. KLUBERG, *Convergence rate for a curse-of-dimensionality-free method for a class of HJB PDEs*, SIAM Journal on Control and Optimization, 48 (2009), pp. 3052–3079.
- [70] X. MENG AND G. E. KARNIADAKIS, *A composite neural network that learns from multi-fidelity data: Application to function approximation and inverse PDE problems*, Journal of Computational Physics, 401 (2020), p. 109020.
- [71] T. NAKAMURA-ZIMMERER, Q. GONG, AND W. KANG, *Adaptive deep learning for high-dimensional Hamilton–Jacobi–Bellman equations*, SIAM Journal on Scientific Computing, 43 (2021), pp. A1221–A1247, <https://doi.org/10.1137/19M1288802>, <https://doi.org/10.1137/19M1288802>, <https://arxiv.org/abs/https://doi.org/10.1137/19M1288802>.
- [72] T. NAKAMURA-ZIMMERER, Q. GONG, AND W. KANG, *QRnet: Optimal regulator design with LQR-augmented neural networks*, IEEE Control Systems Letters, 5 (2021), pp. 1303–1308, <https://doi.org/10.1109/LCSYS.2020.3034415>.
- [73] K. N. NIARCHOS AND J. LYGEROS, *A neural approximation to continuous time reachability computations*, in Proceedings of the 45th IEEE Conference on Decision and Control, Dec 2006, pp. 6313–6318, <https://doi.org/10.1109/CDC.2006.377358>.
- [74] D. ONKEN, L. NURBEKYAN, X. LI, S. W. FUNG, S. OSHER, AND L. RUTHOTTO, *A neural network approach for high-dimensional optimal control*, arXiv preprint arXiv:2104.03270, (2021).
- [75] C. PARZANI AND S. PUECHMOREL, *On a Hamilton-Jacobi-Bellman approach for coordinated optimal aircraft trajectories planning*, Optimal Control Applications and Methods, 39 (2018), pp. 933–948.
- [76] M. RAISSI, P. PERDIKARIS, AND G. E. KARNIADAKIS, *Physics-informed neural networks: A deep learning framework for solving forward and inverse problems involving nonlinear partial differential equations*, Journal of Computational Physics, 378 (2019), pp. 686–707.
- [77] A. V. RAO, *A survey of numerical methods for optimal control*, Advances in the Astronautical Sciences, 135 (2009), pp. 497–528.
- [78] C. REISINGER AND Y. ZHANG, *Rectified deep neural networks overcome the curse of dimensionality for nonsmooth value functions in zero-sum games of nonlinear stiff systems*, Analysis and Applications, 18 (2020), pp. 951–999, <https://doi.org/10.1142/S0219530520500116>, <https://doi.org/10.1142/S0219530520500116>, <https://arxiv.org/abs/https://doi.org/10.1142/S0219530520500116>.
- [79] D. R. ROBINSON, R. T. MAR, K. ESTABRIDIS, AND G. HEWER, *An efficient algorithm for optimal trajectory generation for heterogeneous multi-agent systems in non-convex environments*, IEEE Robotics and Automation Letters, 3 (2018), pp. 1215–1222.
- [80] I. M. ROSS AND M. KARPENKO, *A review of pseudospectral optimal control: From theory to flight*, Annual Reviews in Control, 36 (2012), pp. 182–197, <https://doi.org/https://doi.org/10.1016/j.arcontrol.2012.09.002>, <https://www.sciencedirect.com/science/article/pii/S1367578812000375>.
- [81] V. R. ROYO AND C. TOMLIN, *Recursive regression with neural networks: Approximating the HJI PDE solution*, arXiv preprint arXiv:1611.02739, (2016).
- [82] A. RUCCO, G. NOTARSTEFANO, AND J. HAUSER, *An efficient minimum-time trajectory genera-*

- tion strategy for two-track car vehicles*, IEEE Transactions on Control Systems Technology, 23 (2015), pp. 1505–1519.
- [83] A. RUCCO, P. SUJIT, A. P. AGUIAR, J. B. DE SOUSA, AND F. L. PEREIRA, *Optimal rendezvous trajectory for unmanned aerial-ground vehicles*, IEEE Transactions on Aerospace and Electronic Systems, 54 (2017), pp. 834–847.
- [84] J. SIRIGNANO AND K. SPILIOPOULOS, *DGM: A deep learning algorithm for solving partial differential equations*, Journal of Computational Physics, 375 (2018), pp. 1339 – 1364, <https://doi.org/10.1016/j.jcp.2018.08.029>.
- [85] S. SPEDICATO AND G. NOTARSTEFANO, *Minimum-time trajectory generation for quadrotors in constrained environments*, IEEE Transactions on Control Systems Technology, 26 (2017), pp. 1335–1344.
- [86] E. TODOROV, *Efficient computation of optimal actions*, Proceedings of the national academy of sciences, 106 (2009), pp. 11478–11483.
- [87] I. YEGOROV AND P. M. DOWER, *Perspectives on characteristics based curse-of-dimensionality-free numerical approaches for solving Hamilton–Jacobi equations*, Applied Mathematics & Optimization, (2017), pp. 1–49.
- [88] Z. ZHANG, Y. SHIN, AND G. E. KARNIADAKIS, *GFINNs: GENERIC formalism informed neural networks for deterministic and stochastic dynamical systems*, arXiv preprint arXiv:2109.00092, (2021).
- [89] M. ZHOU, J. HAN, AND J. LU, *Actor-critic method for high dimensional static Hamilton–Jacobi–Bellman partial differential equations based on neural networks*, arXiv preprint arXiv:2102.11379, (2021).